Long-term effects of conventional tillage and no-tillage on saturated and near-saturated hydraulic conductivity – Can their prediction be improved by pore metrics obtained with X-ray CT?

Steffen Schlüter[1], Lukas Albrecht[1], Kai Schwärzel[2,3], Janis Kreiselmeier[2,4]

1. Department of Soil System Sciences, Helmholtz-Centre for Environmental Research – UFZ, Halle, Germany
2. Institute for Integrated Management of Material Fluxes and of Resources - UNU-FLORES, United Nations University, Dresden, Germany
3. Thünen Institute of Forest Ecosystems, Eberswalde, Germany
4. Institute of Soil Science and Site Ecology, TU Dresden, Tharandt, Germany

Keywords: X-ray tomography; hood infiltrometer; tension disc infiltrometer; Stokes-Brinkmann solver; preferential flow; pedo-transfer functions

Abstract

Tillage practices have a profound impact on soil structure and soil hydrology, which may affect ecosystem functions like plant productivity. There is an ongoing debate whether a conversion from conventional tillage (CT) to no-till (NT) leads to an increase in (near-)saturated hydraulic conductivity. This is because true effects are often disguised by large spatial and temporal variability, but also by the deficiencies in the measurement technique.

In this paper, we measured (near-) saturated hydraulic conductivity (K_s and K_{-2}) in a long-term tillage trial (26 years) in Germany with three different methods: hood infiltrometer (HI) in the field, tension disk infiltrometer (TI) on undisturbed soil cores and direct simulation (DS) of water flow on X-ray CT images of macropore structure in these soil cores with a Stokes-Brinkmann solver. On average the absolute values varied by two orders of magnitude in the order TI < HI < DS with very low correlation (R^2<0.05) between $\log_{10}(K_s)$ measurements. The conversion from CT to NT caused an increase in bulk density, a decrease in air capacity and a small but consistent decrease in grain yields. K_s was increased when measured with HI but decreased in TI and indifferent when measured with DS. This inconsistency is caused by the proportion at which large biopores that are more frequent in NT soil due to higher earthworm abundance contribute to total flow in each measurement technique. Regression analyses between pore space attributes measured with X-ray CT and K_s (and K_{-2}) showed very strong agreement with DS values, but poorer agreement with HI and TI, suggesting that those values are afflicted with measurement artifacts like poor contact, entrapped air, different average volumes and so on.

The pore metric with highest predictive power (>90%) on simulated K_s in NT soil cores was the critical pore diameter because it represents the bottleneck that restricts a large contribution to flow by elongated biopores. However, in plowed soil (CT) pore metrics that best describe flow through the loose soil matrix, like macroporosity and pore connectivity, have a higher predictive power and the critical

pore diameter is rendered meaningless. The relative importance of various pore metrics as good predictors of hydraulic conductivity does not only change in a very small pressure range (K_s vs. K_{-2}) but also between measurement techniques (HI vs. TI vs. DS). These inconsistencies raise the question if and how existing pedo-transfer functions for estimating (near-) saturated hydraulic conductivities can be extended by image-derived pore metrics in a meaningful way.

1. Introduction

The change from conventional to conservation agriculture has many implications for ecosystem functions like water filter and storage, carbon storage and plant production (Palm et al., 2014). There is a whole range of tillage intensities, starting from conventional tillage with a moldboard plow that turns the soil in the plow layer, to reduced (or minimum) tillage with a cultivator or disk harrow that loosens the soil superficially, to no-till or direct drilling, as well as combination thereof in strip tillage (Licht and Al-Kaisi, 2005; Pöhlitz et al., 2018; Tebrügge and Düring, 1999). The farmer's choice on tillage intensity is usually driven by economic interests in terms of expected yields, investments in machinery, agrochemicals fuel and labor costs, but also entails ecological consequences, e.g., in terms of soil degradation, erosion and carbon sequestration (Palm et al., 2014; Soane et al., 2012).

The lack of plowing has direct and indirect consequences on soil structure. Usually soil compaction sets in with the conversion to no-till, which can lead to a reduction in air capacity and an increase in bulk density and penetration resistance in the topsoil (Abdollahi et al., 2017; Abdollahi and Munkholm, 2017; Rasmussen, 1999; Rücknagel et al., 2017). However, these trends may vanish when comparing tillage trials across different climates, textures and time scales (Blanco-Canqui and Ruis, 2018). The status of soil physical properties of a NT-system may for example be dependent on the time passed since its establishment (Reichert et al., 2016). Initially macroporosity decreases, while bulk density and microporosity increases. After several years this may reverse through a re-structuring of the soil by bioturbation. Legacy effects also exist for reverse conversion, i.e., a topsoil that is plowed once after a period of conservation tillage has different soil physical properties than continuously plowed topsoils (Kuhwald et al., 2017).

Apart from bulk properties, tillage also affects pore morphology. Tillage forms soil clods, i.e., chunks of intact soil in which the older soil structure is conserved, that are embedded in a loose, broken up soil matrix with isotropic pores and increased meso to macroporosity (Dal Ferro et al., 2014; Kravchenko et al., 2011; Schlüter et al., 2018). Tillage destroys continuous biopores, whereas no-till leads to the buildup of elongated biopores through root growth and earthworm activity that become partially re-filled over time (Lucas et al., 2019; Peth et al., 2008). An indirect effect of tillage on soil structure is the accumulation of soil organic carbon in the first 10cm of the topsoil under no-till (Blanco-Canqui and Ruis, 2018; Tebrügge and Düring, 1999), which leads to a higher soil structure stability and in combination with higher antecedent bulk density to a lower susceptibility to soil compaction (Rücknagel et al., 2017).

Changes in the pore structure have direct consequences for water retention in mesopores as well as fast water flow and aeration through macropores. The effect of tillage intensity on infiltration capacity and saturated hydraulic conductivity has been intensively studied, but there is no consensus on general trends (Strudley et al., 2008). Preferential flow through the macropore network may (Lipiec et al., 2006;

Pagliai et al., 2004) or may not (Kahlon et al., 2013; Vogeler et al., 2009) increase under no-till depending on whether the higher degree of bioturbation and preservation of biopores can compensate for the loss in macroporosity due to soil compaction. Very often, notoriously high spatial and temporal variability disguised trends in hydraulic conductivity caused by tillage intensity (Alletto and Coquet, 2009; Buczko et al., 2006; Jirků et al., 2013; Rienzner and Gandolfi, 2014; Schwen et al., 2011; Strudley et al., 2008).

Another reason for mixed results across studies about tillage effects on saturated and near-saturated hydraulic conductivity is uncertainty in the measurement itself (Morbidelli et al., 2017). There are several techniques to conduct infiltration experiments in the field or on undisturbed soil cores at full saturation or low suction such as tension disk infiltrometers (Perroux and White, 1988), hood infiltrometers (Schwärzel and Punzel, 2007) or the Guelph permeameter (Reynolds and Elrick, 1985). Due to the different approaches to bring the infiltrating water in contact with the soil, different strategies to prevent surface sealing and pore clogging, different soil volumes that are probed by the infiltration front or sampling artifacts in soil cores like wall disturbances, differences in derived conductivities of more than one order of magnitude have been reported (Fodor et al., 2011; Reynolds et al., 2000; Schwärzel and Punzel, 2007).

Until recently there was no way to disentangle true pore structure effects from deficiencies in the infiltration measurements. With the advent of non-invasive imaging of soil structure with X-ray computed tomography (X-ray CT) and direct simulation of water flow on 3D soil structure images with massively parallel computing (Andrä et al., 2013; Blunt et al., 2013) it should be possible to determine the resistance that the original soil structure imposes on water flow and distinguish it from measurement artifacts like air entrapment and wall effects.

X-ray CT analysis of undisturbed soils cores have paved the way to assess soil structure through pore space characterization and to disregard the concept of soil aggregates altogether (Rabot et al., 2018). This quantitative description of soil structure has also been identified as a chance to improve pedo-transfer functions (PTF) for hydraulic conductivity (Van Looy et al., 2017; Vereecken et al., 2010; Zhang and Schaap, 2019), i.e., to amend its prediction based on models with easily available soil properties like texture, bulk density and organic carbon content with structural properties. As we will show, despite having the same texture and higher bulk density no-till soils may have higher saturated conductivity than tilled soils, when macropore flow through large continuous, biopores occurs. Accounting for macropore features in future PTFs requires to (1) identify the most promising structural metrics to predict flow, (2) to initiate large databases in which hydraulic properties and structural properties are stored together and (3) to get a better understanding of the uncertainty that comes with predictions based on structural properties and the uncertainty that comes with the measurement itself. Picking up the recent work of other groups (Koestel et al., 2018; Zhang et al., 2019), this study was our first step into this direction

The main objective of this study was to investigate tillage effects on macropore structure, saturated and near-saturated conductivity. The study was carried out on a long-term tillage trial (26 years) in Southeast Germany and compared non-tilled with plowed topsoils. Hydraulic measurements were conducted with hood infiltrometers in the field, with tension disc infiltrometers on undisturbed soil cores that were scanned with X-ray CT and with direct simulation of water flow on the resulting macropore structure. Another aim of this study was to explore how well the pore structure attributes derived from X-ray tomography are suited to predict saturated and near-saturated hydraulic conductivity measured with different methods. Our hypotheses were that (i) the predictive power of pore structure attributes should be highest on simulated conductivities, as these are based on exactly the soil core volume and are free of measurement artifacts. (ii) Furthermore, if the set of attributes fully captures the structural properties that govern water flow, then their predictive power should be equally high for both tillage treatments.

2. Material and Methods

2.1. Field trial description

The long-term field trial is located in Lüttewitz, Germany (51°7’6N, 13°13’43E, 275 m.a.s.l.) and receives a mean annual precipitation of 643 mm with a mean annual temperature of 8.1 °C (Schmidt et al., 2002). The soil type is a Haplic Luvisol (German: Parabraunerde) on loess deposits. The field trial was established in 1992 and is composed of four tillage treatments in large parallel strips between 5.4 and 7.8 ha: 1. conventional tillage (CT) with a moldboard plow (up to 30 cm depth), 2 .deep mulch tillage, 3. shallow mulch tillage, 4. no-tillage (NT). In this study only the CT an NT treatments are investigated. The three-year crop rotation comprised sugar beet in the first year (*Beta vulgaris*), followed by two years of winter wheat (*Triticum aestivum*). Seedbed preparation on CT before winter wheat and sugar beet was done with a cultivator down to 10 cm. On NT, a shallow seedbed (3-5 cm) cultivation was only done before sugar beet to ensure the establishment of the crop (Koch et al., 2009). Sampling was carried out in spring 2018 in winter wheat (after sugar beet), seven months after the last plowing in the CT treatment. The trial has no replicated plots, but all locations were situated on flat terrain and had very similar silt loam texture (CT - 18% clay, 78% silt, 4% sand; NT - 20% clay, 77% silt, 3% sand). The bulk density measured in 10cm depth was higher in the NT strip (1.53 ± 0.05) as compared to the CT strip (1.40 ± 0.06) and coincide with previously reported values (Jacobs et al., 2015). Organic carbon (C_{org}) and total nitrogen (N) contents in that depth were only slightly higher on the NT strip (C_{org} 1.28 %, N 0.14%) compared to CT (C_{org} 1.21 %, N 0.13%). Across the profile C_{org} and N contents are more evenly distributed on the tilled soil while on NT there is a stratification with an accumulation on the soil surface (Andruschkewitsch et al., 2013).

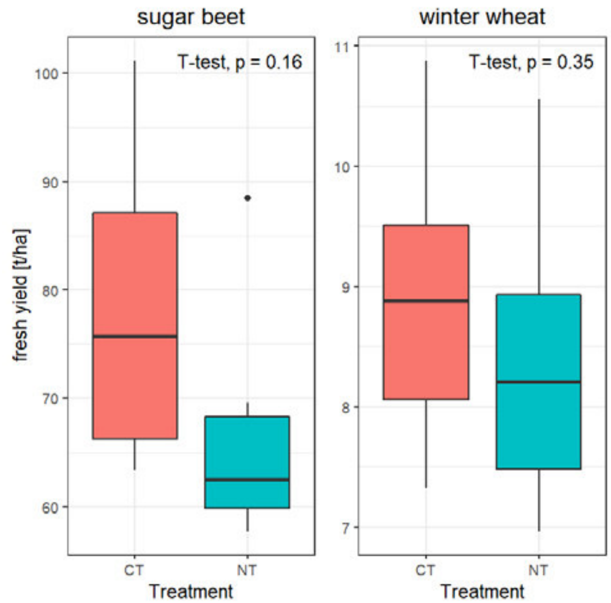

Figure 1: Yield data for sugar beet (n=6) and winter wheat (n=11) in the plots with conventional tillage (CT) and no-tillage (NT). The record comprises all years from 2002 to 2018.

On average, both winter wheat and sugar beet yields were higher on CT compared to NT. From 2002 to 2018 winter wheat yielded 9.1 t ha^{-1} on the tilled plot while the untilled plot yielded 8.6 t ha^{-1} (both 85% dry matter). For the same time frame, sugar beet yields amounted to 78.3 t ha^{-1} on the CT and 66.7 t ha^{-1} on the NT plot (taproot fresh matter). For both crops the differences were not significant due to considerable variations in yield between years. Average yields in the reduced tillage plots ranged in between NT and CT (data not shown).

In the absence of tillage both deep-dwelling (anecic), i.e., *Lumbricus terrestris*, and laterally moving (endogeic) earthworm species, i.e., *Aporrectodea caliginosa*, *A. rosea* and *Allolobophora chlorotica*, were more abundant (October 2000: CT – 60, NT – 255, April 2001: CT – 45, NT – 102 Ind. m^{-2}) and had a higher biomass (October 2000: CT – 30, NT – 225, April 2001: CT – 25, NT – 130 g m^{-2}) compared to CT (Schmidt et al., 2002). This is in line with observations from other long-term tillage trials in that region with similar soil texture (Schlüter et al., 2018; Ulrich et al., 2010). This has implications for bioturbation and consequently soil structure on both plots which will be addressed in this study.

Undisturbed soil cores (ø: 10 cm, h: 10 cm) were acquired with a rotating sampling device (Kuka et al., 2013) (UGT GmbH, Germany) directly underneath the infiltration experiment in a depth of 10-20cm in the drained soil two days after infiltration. The soil cores were wrapped in air-tight bags to reduce evaporation and stored at 4°C to reduce biological activity prior to X-ray tomography analysis. Smaller soil cores ($100cm^3$) were acquired in the direct vicinity of the infiltration experiments for bulk density measurements.

2.2.(Near-)Saturated hydraulic conductivity and water-conducting porosity

Thirteen sampling locations for hood infiltrometer (HI) measurements were chosen in each treatment with a spacing of approx. 50m in between. The HI measurements (IL 2700, UGT GmbH, Germany) were carried out at pressure heads (h) of 0 and then repeated at -2cm on the same location. At least half a reservoir had to be infiltrated or 10min had to pass to move to the next pressure head. Readings were done every 30 s and steady state was assumed after water level decline in the reservoir did not differ by more than 2 mm for three consecutive steps.

Infiltration data was analyzed using the piecewise linear interpolation procedure by Reynolds and Elrick (1991). This procedure is based on the analytical solution for 3D infiltration from a circular source with constant pressure head h by Wooding (1968). Hydraulic conductivity was estimated at the measured h and at their midpoint. As the hood infiltrometer could not always be set to exactly the required h the Gardner (1958) exponential model was used to obtain hydraulic conductivity at h=0 and -2 cm (K_s, K_{-2}).

Hydraulic conductivity at pressure heads of 0 and -2 cm was measured in this order directly on the soil cores with custom-made tension disc infiltrometers (TI) (Perroux and White, 1988) that exactly fit the inner diameter of the core. The measurements were done after X-ray tomography. The soil cores were saturated from below without vacuum application for 24 hours by placing them in a water bath with a table slightly lower than the core height. This choice against vacuum applications entails more air entrapment, but is closer to the field conditions, were air entrapments are also realistic. The wet soil cores were then placed on a sand bed in which the pressure head was adjusted to the corresponding value of the disc infiltrometer with a hanging water column. The soil surface was filled with a thin sand layer (grain size 0.7-1.2 mm) to improve contact and the bottom of the soil core was supported with a coarse nylon mesh (mesh size 1mm) to prevent soil loss.

2.3.X-ray tomography and image analysis

Soil cores were scanned with X-ray tomography (X-tek XCT 225, Nikon Metrology) at an energy of 180 kV and beam current of 280 µA and a 1.2 mm Cu filter for beam hardening reduction. 2800 projections were acquired with one frame per projection and an exposure time of 700 ms each. The projections were reconstructed into a 3D tomogram with a filtered back projection algorithm in X-tex CT Pro. The spatial resolution was 60 µm and the gray scale resolution was 8-bit. The darkest and brightest 0.2% of voxels were set to 0 and 255, respectively, with linear stretching in between.

The raw images were filtered with a 3D non-local means filter (Tristán-Vega et al., 2012) using stand-alone software (https://www.nitrc.org/projects/unlmeans/). A vertical drift in the mean gray values that is caused by the X-ray CT hardware was corrected with a script written in Quantim (Schlüter et al., 2016). Segmentation into pores and background was carried out with simple thresholding using the average of several histogram-based thresholding methods after outlier removal as implemented in Quantim (Schlüter et al., 2014). The segmented pore space was differentiated into big pores (d > 1.48 mm) that are drained at h=-2 cm and the remaining macropores that remain water-filled (Figure 2b). This was achieved by employing the 'Local Thickness' method in Fiji/ImageJ, which stores the diameter of the largest sphere that fully fits into the pore space at this voxel location, followed by thresholding at the given pore diameter. This spatial distribution of entrapped air is only hypothetical and based on invoking Young-Laplace law, which typically does not resemble air clusters in wet soil (Pot et al., 2015), as their shape and position would also depend on air continuity, wettability and the wetting history.

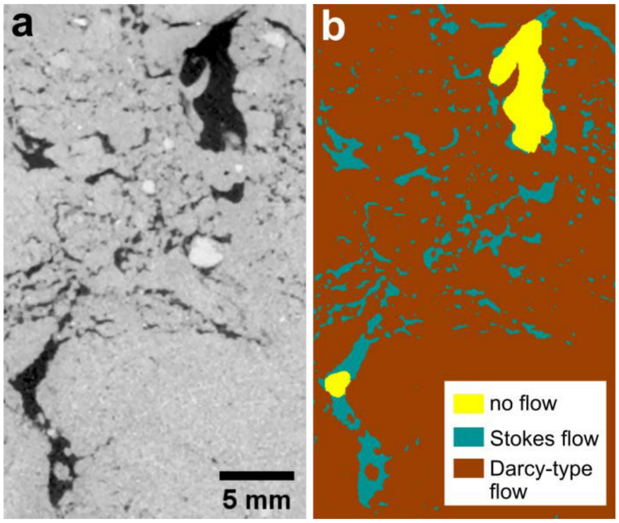

Figure 2: (a) 2D slice of a X-ray CT scan after non-local means filtering. (b) Processed image after image segmentation and pore diameter thresholding: porous matrix (brown), water-filled pores (blue), air-filled pores (yellow).

Several pore space attributes were computed on the segmented images using Fiji/ImageJ (Schindelin et al., 2012): 1. Macroporosity or visible porosity larger than 60µm (mp) was derived from voxel counting. 2. The critical macroporosity (cmp) was determined as the minimum macroporosity in the direction of flow, by sectioning the soil core into horizontal layers of ten voxels (0.6 mm). 3. Pore distance histograms were derived from the 3D Euclidean distance map in soil. That is, the shortest distance to a macropore voxel is stored in each soil matrix voxel. The average pore distance (dist) is derived from this pore distance histogram. 4. Pore diameter histograms were derived from the Local Thickness map. The average pore diameter (apd) is derived from this pore diameter histogram. 5. The critical pore diameter (cpd) was determined with the SoilJ plugin for Fiji/ImageJ (Koestel, 2018). It corresponds to the bottleneck in the percolating pore clusters that connect the top and bottom boundaries of the image. 6. The Γ indicator (conn) is derived from the size distribution of individual pore clusters resulting from Connected Components labeling in the MorpholibJ plugin of Fiji/ImageJ (Legland et al., 2016). This connectivity indicator Γ quantifies the connection probability between two randomly chosen pore voxels. It is one if all pore voxels are connected in one big cluster and approaches zero if the pore space is very fragmented (Jarvis et al., 2017; Renard and Allard, 2013).

This selection of pore space attributes has been carefully curated for this study due to their reported ability to predict flow based on theoretical considerations, e.g., mp as a term in the Kozeny-Carman equation (Zhang and Schaap, 2019), cpd as a cornerstone in percolation theory and critical path analysis (Katz and Thompson, 1986; Koestel et al., 2018), or cmd for being a proxy for the harmonic mean of permeabilities that can be expected for heterogeneity perpendicular to the flow direction (Renard and De Marsily, 1997). In addition, several empirical studies have shown that the selected set of pore space attributes or a subset of it performed better than other image-derived attributes to predict saturated or near-saturated flow (Koestel et al., 2018; Paradelo et al., 2016; Zhang et al., 2019)

2.4. Direct simulation of saturated hydraulic conductivity

Saturated and near-saturated water flow was modeled by direct simulation (DS) on the segmented X-ray CT images with a Stokes-Brinkmann solver as implemented in the FlowDict module of Geodict (Revision

31172, Math2Market GmbH, Germany). The LIR solver (Linden et al., 2015) with an adaptive finite volume grid was used to calculate the steady-state flow field and derive saturated hydraulic conductivity as well as near-saturated hydraulic conductivity at h=-2cm, for which the largest pores were blocked by air (Figure 2b). The finite volume approach in combination with adaptive grid methods requires significantly less memory than comparable Lattice-Boltzmann methods. In this way it was possible to use the entire, undisturbed part of the soil core at the original resolution (60µm) as a model domain (1530 x 1530 x 1450 voxels). The Stokes-Brinkmann equations allow for a coupling between fast, laminar Stokes flow in the segmented pore space and slow Darcy-type flow through the porous soil matrix (Figure 2b). Periodic boundary conditions in flow direction were used including a 2 mm thick redistribution layer at the top and bottom of the model domain. The effective hydraulic conductivity of the soil matrix was set to 8.5 cm/d (permeability 10 mD), a typical value derived from pedo-transfer functions for this texture and a bulk density of 1.65 g/cm³ (Ad-hoc-AG Boden, 2005; Schaap et al., 2001). This matrix density was estimated by extrapolating the data from image-derived macroporosity and measured bulk density to zero macroporosity. A sensitivity analysis showed that a reduction of this matrix conductivity by an order of magnitude (1 mD) had virtually no effect on effective conductivity of the entire core and an increase by one order of magnitude (100 mD) only increased effective conductivity by less than 5%. This is because a decrease in background conductivity funnels more flow through the macropore system and vice versa.

2.5. Statistical analysis

The software R, version 3.5.3 (R: The R Project for Statistical Computing) was used for the statistical evaluation of the data. All measured properties were tested for normal distribution using the Shapiro-Wilk test. Macroporosity, critical macroporosity, average pore size, average pore distance, water-conducting porosity, as well as the logarithm of the saturated conductivity of the direct simulation were not normally distributed. A T-test (normally distributed data) or a Mann-Whitney-U-test (non-normally distributed data) was performed to test for significant differences in the mean of both treatments.

The correlation of the pore space attributes (independent variable) with the hydraulic conductivities (dependent variable) was carried out with Spearman rank correlation coefficients, since the relationships are not necessarily linear. In addition, a partial least square regression (PLSR) implemented in the *pls* package (Mevik, 2016) resulted in the percentage of variance in the dependent variable that is explained by the independent variables. Since PLSR assumes normal distributions, the values with metric units (sizes and distances) were transformed using a logarithmic transform and ratios between 0 and 1 (porosity, connectivity and critical macroporosity) were transformed with a logistic function. All data ranges were standardized by a z-transform (zero mean and standard deviation of one).

Coefficients of determination R^2 and regression lines shown in the figures were generated by the *ggpmisc* package.

3. Results

3.1. Hydraulic properties

Despite the higher bulk density in NT strip as compared to the CT strip the non-tilled soil exhibits a trend ($p<0.1$) towards larger saturated hydraulic conductivities when measured with a hood infiltrometer at the soil surface (Table 1). The difference becomes even more significant ($p<0.05$) when measured at h=-2 cm.

The hydraulic conductivities at a given pressure head were substantially lower when measured with tension disk infiltrometers directly on the soil cores taken from a soil depth of 10-20cm instead HI measurements at the soil surface. Note that the bulk density was reported to increase with depth from 1.35 g/cm³ (0-10cm) to 1.41 g/cm³ (10-20cm) in the CT strip and from 1.44 g/cm³ (0-10cm) to 1.52 g/cm³ (10-20cm) in the NT strip (Jacobs et al., 2015). A very conservative estimate of the HI front depth from the amount of infiltrated water, antecedent water content and piston flow assumption amounts to 19 and 33cm on average for CT and NT, respectively. So the HI measurements should have partially or fully included most of the soil core volume used for TI. Since the infiltration front in the field is more irregular it likely reached beyond the sampled depth (10-20cm) also in the CT soil and might have been affected by the plow pan and undisturbed soil structure underneath it, both of which have a higher bulk density (CT: 20-30 cm: 1.46g/cm³, 30-45cm: 1.55 g/cm³, Jacobs et al. (2015)) than the plow horizon sampled with TI and therefore exert a higher resistance to flow. Furthermore, the order is reversed between tillage treatments in the TI data. There is a trend towards lower $\log_{10}K_s$ ($p<0.1$) and significantly lower conductivities at h=-2cm ($p<0.001$) in NT soil cores.

The saturated hydraulic conductivity obtained with direct simulation on the segmented X-ray CT image of the pore space is by far the highest of all methods and on average more than one order of magnitude larger than those obtained with infiltrometers. There is no significant difference in simulated $\log_{10}(K_s)$ between the tillage treatments. On average near-saturated hydraulic conductivity drops by one order of magnitude in NT soil cores as compared to K_s, whereas there is hardly any change in CT soil cores. This causes a significantly lower $\log_{10}(K_{-2})$ in non-tilled soils ($p<0.05$).

Table 1: Hydraulic conductivities of measured with different methods in the conventional tillage (CT) and no-till (PT) plots (n=13). Test results for significant differences are displayed in the row header (* - p<0.001, ** - p<0.01, * - p<0.05, ° - p<0.1, NS – not significant).**

technique	property	Treatment	Mean	SD
HI - Hood Infiltrometer	$\log_{10}K_s$ ° [cm d^{-1}]	CT	2.89	±0.24
		NT	3.07	±0.19
	$\log_{10}K_{-2}$ * [cm d^{-1}]	CT	2.71	±0.25
		NT	2.91	±0.16
TI - Tension Disk Infiltrometer	$\log_{10}K_s$ ° [cm d^{-1}]	CT	2.46	±0.22
		NT	2.14	±0.60
	$\log_{10}K_{-2}$ *** [cm d^{-1}]	CT	1.95	±0.30
		NT	1.36	±0.48
DS - Direct Simulation	$\log_{10}K_s$ NS [cm d^{-1}]	CT	4.11	±0.44
		NT	4.37	±0.82
	$\log_{10}K_{-2}$ * [cm d^{-1}]	CT	4.03	±0.26
		NT	3.25	±0.15

The correlation between all three saturated hydraulic conductivities on a sample level is very low (Figure 3), with R^2<0.05 for all combinations of methods and tillage treatments. A pertinent pattern in saturated hydraulic conductivity derived from direct simulation is that NT cores are grouped into small values ($\log_{10}K_s$ <4.2) and large values ($\log_{10}K_s$ >5.0) presumably depending on whether there exists are large continuous biopore in the direction of flow, whereas all other combinations of methods and tillage treatment evoke normality in the residuals around the means.

The correlations between the three techniques are somewhat higher ($0.1 < R^2 < 0.3$) for near-saturated hydraulic conductivities of individual tillage treatments (Figure 2). Pooling the treatments leads to a higher coefficient of determination (R^2=0.43) between DS and TI, but not between DS and HI (R^2=0.03).

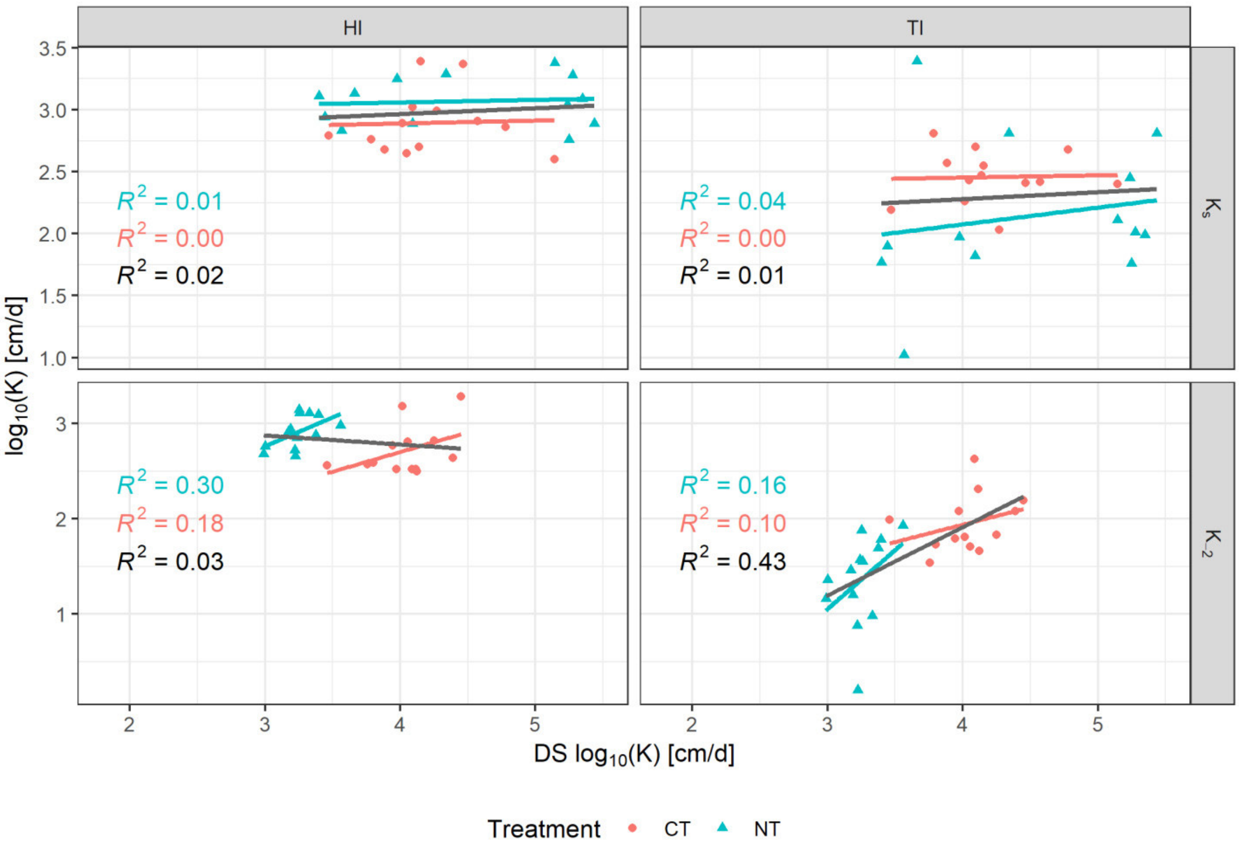

Figure 3: Log-transformed saturated hydraulic conductivities (K_s) and near-saturated hydraulic conductivities (K_{-2}) derived from hood infiltrometers in the field (HI), tension disc infiltrometers on intact soil samples (TI) and direct flow simulations on the 3D pore structure (DS). Note the different scale for the three measurement types.

3.2. Visual assessment

A typical sample with pore structure properties close to the average of each tillage treatment is visualized in Figure 4. The effect of plowing or the lack thereof is clearly visible in the X-ray CT images. Plowing leads to a loose matrix with embedded clods, in which the structure prior to plowing is conserved (Figure 3a). Root channels are clearly visible as dark spots in dense clods but also exist within the loose matrix. The pore structure in the non-tilled soil is clearly different (Figure 3b). The loose soil matrix is only present in earthworm burrows that are partially refilled with earthworm cast. The top of the core seems to have a higher volume fraction of loose soil matrix (10-13cm depth in the profile) perhaps due to soil structure disturbance during sugar beet harvest. The rest of the soil is mainly composed of a dense matrix with local bulk density that is likely to be even higher than the average bulk density of 1.53g/cm³.

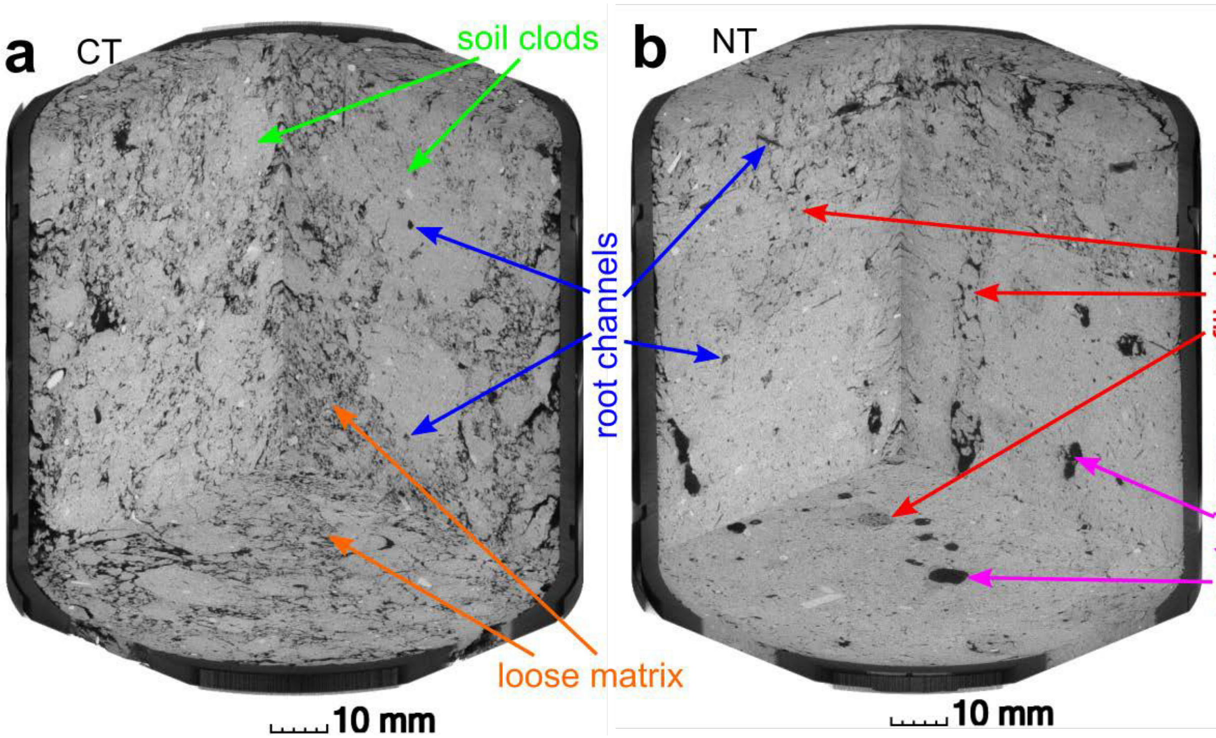

Figure 4: X-ray tomogram cut along three principal plans for one example of (a) plowed topsoil and (b) no-till soil from a depth of 10-20cm each. Salient features are annotated.

3.3. Pore structure attributes

The visual assessment of X-ray tomograms is corroborated by image analysis results (Table 2). The macroporosity in the NT cores is significantly smaller ($p<0.001$), which is in line with the higher bulk density. This lower macroporosity also entails a lower critical macroporosity in the direction of flow ($p<0.001$) and leads to a significantly lower connection probability ($p<0.001$). Interestingly, the average pore diameter is larger ($p<0.001$) in the NT cores, because of a higher contribution from large biopores to total macroporosity, whereas in CT cores the frequency of biopores, cracks and pores in the loose soil matrix with diameters <0.5mm is higher (Figure 5b). This is also reflected in a higher critical pore diameter in NT cores ($p<0.05$). Surprisingly, the average pore distance is the same in both structures despite the different visual appearance and the higher macroporosity in CT soil. Short distances <0.25mm are more frequent in the CT soil due to larger pore surface area contributed mainly by the loose soil matrix (Figure 5b). But this is compensated by a higher frequency of large pore distances >0.75mm in the CT soil which are located in dense clods, so that on average the bulk pore distance is comparable to NT soil with a more even spacing of biopores in an otherwise dense matrix.

Table 2: Image-derived pore structure attributes from the conventional tillage (CT) and no-till (PT) plots (n=13). Test results for significant differences are displayed in the column header (* - p<0.001, ** - p<0.01, * - p<0.05,° p<0.1, NS – not significant).**

Treat-ment	macroporosity*** [-]		critical macro-porosity*** [-]		Γ connectivity*** [-]		average pore diameter*** [mm]		critical pore diameter* [mm]		average pore distance^{NS} [mm]	
	Mean	SD	Mean	SD	Mean	SD	Mean	SD	Mean	SD	Mean	SD
CT	0.15	±0.03	0.10	±0.03	0.90	±0.05	0.28	±0.04	0.61	±0.50	0.37	±0.06
NT	0.07	±0.01	0.04	±0.01	0.68	±0.08	0.56	±0.16	1.26	±0.93	0.38	±0.04

More trends and dependencies among pore structure attributes are revealed by analyzing trends in the scatter and correlation between attributes (Figure 5). There is no correlation between average pore size and macroporosity within a treatment. This low correlation suggests that both properties carry complementary information that in combination may help to explain measured K_s and K_{-2} values better. Pooling the data may lead to the impression that an increase in macroporosity leads to a decrease in average pore diameter (Figure 5a). This is because the gain in macroporosity in CT samples is mainly caused by an increased volume fraction of pores <0.25mm in the loose soil matrix due to plowing (Figure 5b). The very high correlation between connectivity and macroporosity goes to show that both attributes carry redundant information (Figure 5c). The slope is steeper for NT samples as their macroporosities are in the critical range for percolation, whereas CT samples have a well-connected macropore space leading to connection probabilities closer to the theoretical limit of one and therefore generally to a smaller increase in connectivity with increasing macroporosity. The critical macroporosity also exhibits a high correlation with macroporosity, in particular for CT soil cores in which individual layers are fairly representative for the entire core, but less so for NT soil cores in which critical macroporosities are typically reached in very dense layers at the bottom of the cores. The average pore distance decreases with increasing macroporosity in a fairly consistent way for each tillage treatment (Figure 5b) despite the higher macroporosity in CT soil, but the correlation is generally lower than that observed for connectivity and macroporosity. The critical pore diameter is not correlated with macroporosity in either of the treatments, since the volume fraction of macropores has little effect on the bottleneck diameter through the percolating pore cluster.

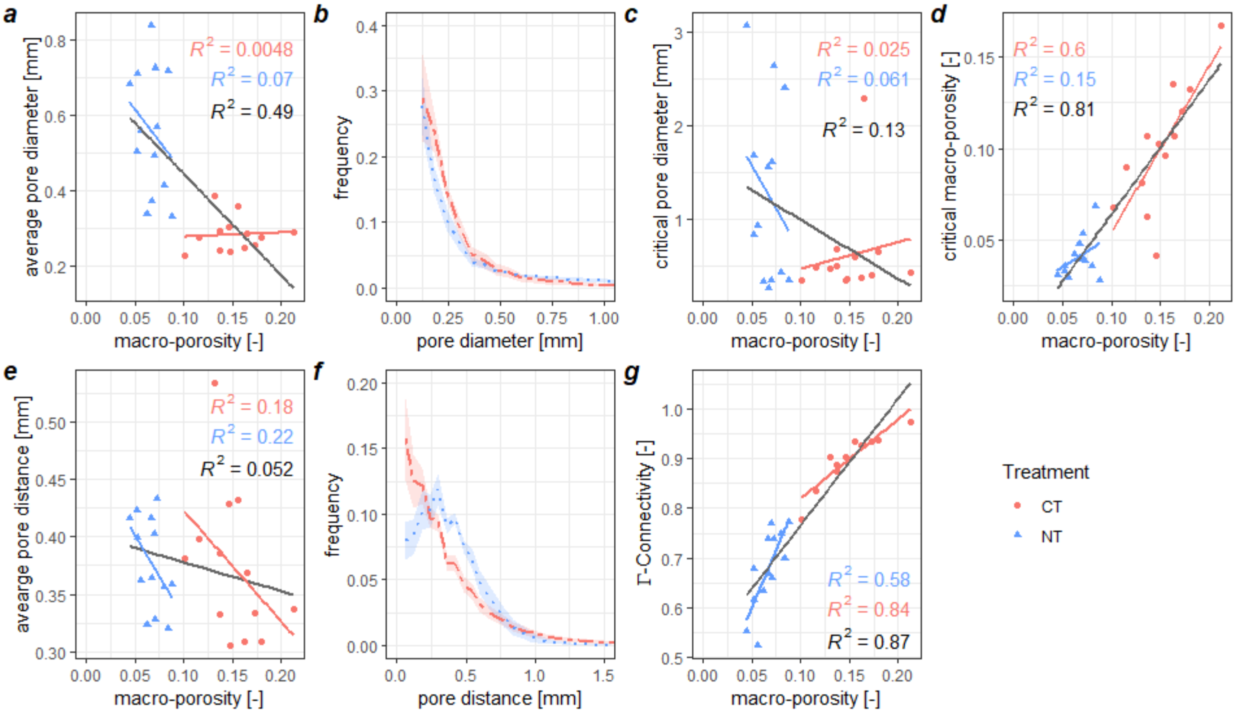

Figure 5: Relationship between different pore structure attributes: (a) average pore size as function macroporosity, based on (b) the pore size histogram. (c) connection probability Γ as a function of macroporosity. (d) average pore distance as a function of macroporosity, based on(e) the pore distance histogram. (f) critical pore diameter as a function of macroporosity.

3.4. Relationship between hydraulic conductivity and pore space attributes

The Spearman rank correlation coefficients between image-derived pore space attributes and (near-) saturated hydraulic conductivity obtained with different techniques (Table 3) exhibit some highly significant correlations, yet with a fairly inconsistent pattern. High correlations may vanish when switching from one tillage treatment to the other (or pooling the data), from saturated to near-saturated hydraulic conductivity or from one technique to the other. Yet, some general deductions may seem valid. First, among all three techniques K-values obtained with DS seem to correlate best with pore space attributes. Second, for DS the most important pore space attribute for K_s values is the critical pore diameter, in particular for NT cores, in which earthworm burrows are the major pathway for flow. That changes for K_{-2} values, when these channels are blocked by air (Figure 2b) and the remaining macropore network conducts the flow, which is best described by macroporosity and pore connectivity. Third, for all three techniques K_{-2} values correlate better with pore space attributes of pooled data than individual tillage treatments. That is, they are more sensitive to the very different flow patterns between CT and NT cores, than to the variability of hydraulic conductivity within a tillage treatment.

Table 3: Spearmen rank correlation coefficients between hydraulic conductivities obtained with different techniques at different pressure heads and pore space attributes derived from X-ray CT images (* - p<0.001, ** - p<0.01, * - p<0.05,° p<0.1).**

property	tech-nique	treat-ment	mp [-]	cmp [-]	conn [-]	apd [mm]	cpd [mm]	dist [mm]
log10K_s	HI	CT	0.24	0.05	0.52 °	0.61 *	0.41	0.46
		NT	0.24	0.03	0.57 *	0	-0.04	0.21

		CT+NT	-0.25	-0.28	-0.11	0.55 **	0.2	0.37 °
		CT	0	0.14	-0.05	0.02	0.09	0.09
	TI	NT	0.29	-0.09	0.39	0.25	0.17	0.05
		CT+NT	0.38 °	0.26	0.39 *	-0.29	0.02	0.01
		CT	0.63 *	0.3	0.62 *	0.35	0.19	-0.13
	DS	NT	0.03	0.24	-0.23	0.84 ***	0.89 ***	0.11
		CT+NT	-0.03	0.05	-0.08	0.48 *	0.78 ***	0.1
		CT	0.08	0	0.35	0.51 °	0.43	0.41
	HI	NT	0.26	-0.04	0.61 *	0.14	0.14	0.31
		CT+NT	-0.37 °	-0.39 *	-0.22	0.62 ***	0.24	0.43 *
		CT	0.25	-0.19	0.21	0.34	0.03	0.21
log10K$_{-2}$	TI	NT	0.16	-0.3	0.57 *	-0.3	-0.37	-0.06
		CT+NT	0.65 ***	0.39 *	0.72 ***	-0.53 **	-0.29	0.04
		CT	0.78 **	0.48 °	0.90 ***	0.51 °	0.18	-0.04
	DS	NT	0.58 *	-0.07 °	0.90 ***	-0.52 °	-0.49 °	0.08
		CT+NT	0.92 ***	0.72 ***	0.97 ***	-0.70 ***	-0.32	-0.08

A general shortcoming of Spearman rank correlations is that they do not indicate the type of relationship between a pore metric and conductivity, i.e., whether it is linear or non-linear. Therefore, it is not possible to assess, whether one is a good predictor for the other and therefore a suitable candidate for deriving pedo-transfer functions.

To do so, requires a partial least regression between pore space attributes and hydraulic conductivities. In Table 4, these results are reported as percentage of variance in the dependent variable (K values) that is explained by the independent variables (pore space attributes). The percentage of explained variance in $\log_{10}(K_s)$ measured with hood infiltrometers is higher for CT soil (72.9%) than for NT soil (43.4%) (Table 2). The explained variability in $\log_{10}(K_s)$ for NT cores is lower either because the core volume (700cm³) is less representative for the pore structure that is encountered by the infiltration front or because the investigated attributes are less adequate for predicting flow in this very different structure. The explained variance is decreased further by pooling all infiltration experiments. Individual simple regressions show that the attribute with the highest predictive power differs among treatments. In CT cores it is the average pore diameter (62.6%) followed by average pore distance (34.7%) and pore connectivity (8.7%). It is safe to assume that saturated flow will mainly occur through the loose matrix produced by plowing. These attributes best describe the channel width within the loose matrix, the volume fraction of the loose matrix (i.e., small pore distances are caused by many small soil fragments in the loose matrix) and the connectivity of pores through the loose matrix, respectively. In NT cores the variability in $\log_{10}(K_s)$ is best described by pore connectivity (34.9%) followed by macroporosity (10%) and average pore distance (6.6%). In NT samples large biopores are supposed to contribute more to saturated flow. In presence of a dense soil matrix, the connectivity of these channels becomes more important for water flow. Especially since the observed connectivities are in the critical range between 0.4 and 0.8, whereas in the CT cores macropore structures are very well connected anyway ($\Gamma > 0.8$). The fact that the macroporosity is in a critical range for percolation in NT cores, but not in CT cores, also explains the higher predictive power of macroporosity on $\log_{10}(K_s)$ for NT. The critical pore diameter does not carry predictive power in either of the treatments, perhaps because a large 3D infiltration front in the field is not constrained by a single pore bottleneck and if so, it might be located outside analyzed soil core.

Table 4: Partial least square analysis resulting in the percentage of variance [%] in $\log_{10}(K_s)$ and $\log_{10}(K_{-2})$ that can be explained with individual pore metrics or all jointly. The color code scales from low (white) to high (green) predictive power.

property	tech-nique	treat-ment	mp [-]	cmp [-]	conn [-]	apd [mm]	cpd [mm]	dist [mm]	joint
$\log_{10}(K_s)$ [cm d^{-1}]	HI	CT	2.2	0.5	8.7	62.6	3.5	34.7	72.9
		NT	11.0	0.1	33.3	0.0	0.1	5.9	43.4
		CT+NT	6.2	7.6	2.0	20.5	4.8	21.1	40.3
	TI	CT	0.0	0.8	0.0	0.1	3.0	1.6	34.3
		NT	3.7	7.2	8.5	0.3	1.0	0.0	65.7
		CT+NT	13.3	4.8	13.5	6.1	0.1	0.0	21.1
	DS	CT	34.2	11.1	33.7	3.6	11.4	4.6	48.4
		NT	3.6	10.9	4.0	78.0	91.4	4.2	94.8
		CT+NT	2.1	0.0	1.1	34.7	66.1	0.1	77.6
$\log_{10}(K_{-2})$ [cm d^{-1}]	HI	CT	0.5	0.0	4.4	60.0	0.2	32.1	74.6
		NT	10.5	0.3	39.9	0.3	0.7	13.3	58.2
		CT+NT	10.3	12.4	4.5	25.8	4.4	23.4	46.6
	TI	CT	6.2	3.6	6.6	4.8	27.1	2.1	67.7
		NT	1.4	14.3	12.0	0.3	2.0	1.5	69.7
		CT+NT	36.9	14.4	40.4	23.7	4.2	0.3	54.4
	DS	CT	72.3	16.7	80.0	29.3	4.0	0.3	95.0
		NT	55.1	0.3	82.4	27.1	27.1	0.1	96.0
		CT+NT	91.7	63.8	95.0	51.9	15.4	0.6	96.5

The explained variance in $\log_{10}(K_s)$ measured by TI is lower for CT cores (34.3%), but higher for NT cores (65.7%) as compared to HI measurements when all pore metrics are considered jointly (Table 2). The explained variance by simple regressions is very low for both tillage treatments, suggesting that the interaction between these pore metrics contributes a large share to the explained variance in the joint PLSR.

The predictive power of pore metrics on $\log_{10}(K_s)$ simulated with a Stokes-Brinkmann solver directly on the 3D pore structure is again very dependent on the tillage treatment (Table 4). For non-tilled soils the predicted variance by all pore space attributes combined amounts to a formidable value of 94.8%, which is almost exclusively based on the critical pore diameter (91.4%). Evidently, water flow in this structure depends mainly on the presence of earthworm burrows and is constrained by the bottleneck along those channels. For tilled soils the explained variance by all pore space attributes combined reaches only 48.4% and is mainly contributed by macroporosity (34.8%) and as consequence of their high correlation also pore connectivity, whereas the critical pore diameter is less relevant for water flow (11.4%). This again supports the idea that the volume fraction of the loose soil matrix is constraining $\log_{10}(K_s)$, which is best captured by bulk macroporosity.

The percentage of explained variance in near-saturated hydraulic conductivities at h=-2cm ($\log_{10}(K_{-2})$) by considering all pore metrics jointly is higher than that of saturated hydraulic conductivity ($\log_{10}(K_s)$) for all measurement techniques and tillage treatments (Table 4). The overall trends are similar to those of the Spearman rank correlation coefficients (Table 3). That is, macroporosity and connectivity replace critical pore diameter as the pore metric with highest predictive power on simulated hydraulic conductivity (DS). For HI and TI measurements the general pattern of which pore metric has the highest predictive power on $\log_{10}(K_{-2})$ for a given tillage treatment is identical to that of $\log_{10}(K_s)$.

4. Discussions

4.1. Predicting saturated hydraulic conductivity

Our findings support the consensus in soil hydrology that saturated hydraulic conductivity is difficult to measure, exhibits a notoriously high spatial variability and is therefore afflicted with a high uncertainty (Fodor et al., 2011; Reynolds et al., 2000; Rienzner and Gandolfi, 2014). For all measurements combined the saturated hydraulic conductivity measured with hood infiltrometers (950 cm/d) was roughly five times higher (Table 1) than measured with tension disc infiltrometers (200 cm/d). This discrepancy between K_s values obtained with hood and tension disc infiltrometers is in a comparable range with previous studies (Matula et al., 2015; Schwärzel and Punzel, 2007) and is mainly ascribed to a better hydraulic contact of the hood compared to the tension infiltrometer (Matula et al., 2015) and disturbances of the soil surface while preparing it for TI measurements. Further, fine particles of the contact material may lead to clogging of pores (Schwärzel and Punzel, 2007). Moreover, hydraulic measurements are known to show hysteretic effects (Clothier and Smettem, 1990) that could have been invoked by saturating the soil cores prior tension disc infiltration whereas HI measurements were conducted directly on field-moist soil. The lack of vacuum when saturating the sample prior to TI measurements could have led to substantial air entrapment. Also, the cores might have been partially drained when quickly moving them from the water bath to the sand bed and this invading air was then additionally trapped during infiltration. Furthermore, we observed slaking and compaction directly underneath the disc infiltrometer. So the measured conductivities might have been more affected by the pore structure of the first mm than by the entire column and macropores underneath might have become disconnected and stayed inactive (Allaire-Leung et al., 2000; Sammartino et al., 2015). In addition, the contact area of the HI (483 cm^2) was larger than the TI (50cm^2), averaged across more vertical heterogeneity and might have sampled the macropore system more representatively. This may also explain why NT cores had a higher K_s and K_{-2} than CT cores when measured with HI, as preferential flow in earthworm burrows contributed more to overall flow and the CT cores were partially affected by the plow pan, whereas the order between tillage treatments was reversed in the TI data, as these large biopores are disrupted by sampling or just not sampled representatively and the effect of the plow pan vanished in the extracted CT cores.

Due to uncertain nature of saturated hydraulic conductivity it has been suggested to put more emphasis on measuring near-saturated hydraulic conductivity and e.g., use K_{-2} as a hinging point to constrain the Mualem model of unsaturated conductivity (Ippisch et al., 2006; Schaap and van Genuchten, 2006). This is supported by our findings (Table 1) as the trends ($p<0.1$) between both tillage treatments turned into significant differences (HI, $p<0.05$) and highly significant differences (TI, $p<0.001$) when considering $\log_{10}(K_{-2})$ instead of $\log_{10}(K_s)$. Likewise, a non-significant difference in $\log_{10}(K_s)$ turned into significantly higher $\log_{10}(K_{-2})$ for CT soil for direct simulations. Finally, the correlation between the three different measurement techniques, though still quite poor ($R^2<0.5$), also improved when switching from $\log_{10}(K_s)$

to $\log_{10}(K_{-2})$ as well as the Spearman rank correlation and partial least square regression between hydraulic conductivity and pore space attributes.

The predicted K_s values derived from direct simulation of saturated water flow on the 3D pore structure allow for an assessment of measurement uncertainties that are usually disguised by bulk measurements. For all measurements combined simulated K_s values are much higher (17400 cm/d) than measured K_s values for both tillage treatments. With a few exceptions (Di Prima et al., 2018) such high values are rarely reported for any kind of infiltrometer. This goes to show that some of the assumption made in the direct simulations of macropore flow under ponded conditions, like complete saturation and perfect wettability are quite unrealistic (Jarvis, 2007). The two order of magnitude discrepancy to tension disc infiltrometer measurements could in addition have been caused by clogging of pores with contact sand and structural deformation of soil structure caused by the TI measurement (Koestel et al., 2018) that all impose a substantial resistance to water flow. The discrepancy to hood infiltrometer measurement is structure-dependent and can be partly ascribed to the vastly different soil volumes that act as a flow domain in DS and HI. The grouping of NT samples into highly conductive and less conductive samples caused by individual biopores in the direct simulation data vanishes in the hood infiltrometer data as a large volume captures the elongated biopores and the bottlenecks that restrict flow more representatively. The absolute values in simulated (DS) and measured (HI) conductivity are similar for less conductive NT samples, suggesting that the small, short-ranged flow paths are representatively captured by a 700cm³ core in these dense soil samples. Likewise, the K_{-2} values in NT cores were similar with both techniques (HI: $\log_{10}K_{-2}$=2.91, DS: $\log_{10}K_{-2}$=3.25; Table 1), as large biopores are blocked by air at h=-2cm. Finally, also hood infiltrometer measurements might be afflicted by pore clogging, air entrapment and soil slaking to some extent.

Even though the Spearman rank correlation analysis occasionally showed very good agreement between pore space attributes and hydraulic conductivities, the partial least square regression analysis revealed that there is little hope in predicting saturated or near-saturated hydraulic conductivity with a universal pedo-transfer function based on a combination of pore structure attributes. This does not mean that the status quo of not considering image-derived macropore features in pedo-transfer functions for K_s estimates at all (Araya and Ghezzehei, 2019; Carsel and Parrish, 1988; Schaap et al., 2001; Vereecken et al., 2010; Wösten et al., 2001), would be the better option. For instance, K_s predictions using only average texture and bulk density data would have led to a vast underestimation for both tillage treatments (CT: 17 cm/d, NT: 8 cm/d; estimated with Rosetta Lite as implemented in Hydrus 1D). It is frequently observed that these PTF estimates of hydraulic conductivity tend to underestimate measured values in the wet range (Vereecken et al., 2010). More recent approaches to identify key factors controlling K_s and K_{-10} in the field have considered additional input parameters beyond texture, bulk density and soil organic carbon, such as land use, season, annual precipitation and temperature as well as experimental conditions like sequence of applied suctions, disk diameter and K estimation method (Jarvis et al., 2013; Jorda et al., 2015). The most important predictors were annual precipitation and temperature for K_{-10} and land use and bulk density for K_s (Jorda et al., 2015) most likely through their impact on soil structure which is the actual controlling factor of hydraulic conductivity but hard to cast in quantitative terms and rarely reported for field studies in a standardized way to be used in large databases.

Here, pore metrics derived from X-ray CT data can contribute a lot to improve PTFs for saturated and near-saturated hydraulic conductivity. But the outcome of our PLSR analysis showed that it is unclear on which pore metric such an extended pedo-transfer function should be based as this changes dramatically between tillage treatments and measurement techniques. The critical pore diameter had an excellent predictive power on simulated $\log_{10}(K_s)$ (explained 91.4% of the observed variability), but only for NT samples in completely saturated soil where the bottleneck in large biopores really imposed the decisive resistance to flow. This confirms recent findings by Koestel et al. (2018) based on infiltration experiments and X-ray CT analysis for a broad selection (n=95) of Norwegian soils that also ascribed the highest predictive power on critical pore diameter. However, in plowed CT soil the predictive power of the critical pore diameter on simulated $\log_{10}(K_s)$ was much lower (11.4%). This change in predictive power between biopore-dominated and matrix-dominated flow confirms recent findings by Zhang et al. (2019). As pointed out by Koestel et al. (2018), the suitability of the critical pore diameter in predicting flow is based on the assumption of a broad distribution of local hydraulic conductivities, which is apparently not justified in more homogenous, tilled soils. In CT soil even the combination of all pore structure attributes left more than half of the observed variability in simulated $\log_{10}(K_s)$ unexplained even though the structure analysis and flow simulation was based on the same volume. It is unlikely that another pore structure metric unaddressed in this study could substantially improve the predictive power, since very often shot-gun approaches that favor a large number of structure parameters over a selected number of targeted, complementary metrics have shown that a large part of them is highly correlated (Larsbo et al., 2014; Müller et al., 2018; Smet et al., 2018), often necessarily so by direct dependencies, and can therefore hardly improve conductivity predictions. The selection of pore space attributes used in our study targeted already those metrics that were identified as the most promising to predict water flow in previous studies (Koestel et al., 2018; Paradelo et al., 2016; Schlüter et al., 2018; Zhang et al., 2019). One way to improve predictions by pore structure attributes could be to divide the domain into several sections in the direction of flow and take the harmonic mean of section averages as predictors of conductivity (Renard and De Marsily, 1997; Wen and Gómez-Hernández, 1996) or only evaluate the pore metrics in the limiting layer (Paradelo et al., 2016; Zhang et al., 2019) to better account for layers with a particularly high flow resistance. Note that this is already partly implemented in this study by accounting for the critical macroporosity in the direction of flow and that this extension would maintain the excellent prediction of conductivity by the critical pore diameter for NT soil cores. Likewise, the assumption of a constant matrix conductivity through unresolved pores for the Strokes-Brinkmann solver might be too strong and could be replaced by a variable matrix conductivity that is coupled to the grayscale in the X-ray CT data (Kang et al., 2019), though our sensitivity analysis showed that the effect on effective conductivity of the core is small. However, it is debatable whether these extensions are warranted since a much larger fraction of unaccounted variability seems to be contributed by deficiencies in the conductivity measurements like air-entrapment, imperfect contact, soil deformation by the measurement or different measurement volumes (Koestel et al., 2018).

In summary, these findings confirm previous recommendations (Zhang and Schaap, 2019) that (1) the development of soil structure-based pedo-transfer functions for hydraulic conductivity might benefit from replacing K_s with near-saturated hydraulic conductivity like K_{-2} as the uncertainty associated with the measurement typically goes down. However, this will also change the order of pore space attributes with the highest predictive power as the largest pores will be blocked by air. (2) When setting up large databases that combine image-derived structural information with measured hydraulic properties, only data with consistent measurement protocols should be incorporated or at least all reported measurement data should be flagged with meta-information on the measurement technique so that data selection can be carried out accordingly prior to training and validation of pedo-transfer functions.

4.2. Ecological relevance of tillage

The increased biopore formation rate through larger earthworm abundance and the better biopore continuity through the lack of plowing caused a trend ($p<0.1$) towards higher saturated hydraulic conductivities in the NT strip that was even more significant ($p<0.05$) for near-saturated hydraulic conductivity at the time of sampling, when measured in the field with hood infiltrometers. However, differences in K_s between both tillage treatments vanished when directly simulated on the three-dimensional pore structure and even changed order when measured with tension disc infiltrometers. Furthermore, repeated hood infiltrometer measurements at this site indicate that when measured over several growing seasons (five occasions with n=5 per occasion and treatment) on average the differences in K_s between CT (750 cm/d) and NT (492 cm/d) are not significant (unpublished data) and often depend on the time of measurement during a cropping season. K_s values vary considerably over time in the CT plot due to tillage and subsequent soil settling, whereas they are more stable over time in the NT plot.

The success of a conversion from conventional tillage to no-till is typically evaluated by its effect on off-site and on-site ecosystem services, of which the most important to farmers is usually crop production but may also include carbon sequestration and resilience to soil degradation. A detrimental effect of no-till for crop production may occur when air capacity falls below a critical value for root penetration and soil aeration due to the lack of soil loosening through plowing. Bulk density in the no-till plot increased to 1.53 g/cm³; a value that is around the critical value (1.55 g/cm³) for root growth restriction in silt loam (Kaufmann et al., 2010). The critical air capacity, i.e., air content at field capacity, for soil aeration is assumed to be 5% (Lebert et al., 2004) to 8-10% (Reichert et al., 2009; Werner and Paul, 1999), which is in the range of macroporosity of the NT soil cores (7%, Table 2). Note that the voxel resolution (60µm) roughly corresponds to the pore diameter with an air entry pressure at field capacity (pF 1.8) and can therefore be used as a proxy for air capacity (Schlüter et al., 2018). All measured K_s values in the NT strip seem to be uncritical for crop production as they exceeded the limiting value for ponding estimated at 10 cm/d (Werner and Paul, 1999), and ponding might not be critical at this site anyway for its terrain and moderate annual precipitation. Direct drilling as practiced on this site has been shown to result in decreasing yields of both sugar beet and winter wheat (Figure 1 and Jacobs et al. (2015)). Winter wheat may still be produced profitably under such a system (Dieckmann, 2008) as the reduction in yield is compensated by the reduced costs for machinery and labor while at the same time the increase in costs for pest management is only marginal (personal communication with the farmer and Rico Rühl, Südzucker). Soil loosening may be warranted for when growing sugar beet (Koch et al., 2009) in order to achieve more favorable rootability, aeration and pest reduction. In fact, no-till poses an economic disadvantage for sugar beet at this site as the yield reduction and increased costs for pest control are more substantial as compared to winter wheat and cannot be compensated by the reduced costs for tillage (personal communication with the farmer and Rico Rühl, Südzucker).

5. Conclusions

Though a non-replicated trial should be interpreted with caution when drawing general conclusion about the effect of tillage treatments on soil functions, our dataset is useful in demonstrating how the lack of plowing changes morphological features of the macropore network and how this affects (near-)saturated hydraulic conductivity. The increase in K_s and K_{-2} caused by a higher abundance of large biopores due to higher earthworm abundance and their preserved continuity in the absence of plowing under no-till was only detected with hood infiltrometer measurements in the field but absent in direct flow simulation on the three-dimensional pore structure of undisturbed soil cores and even reversed in tension disk infiltrometer measurements on those soil cores. Each of the three methods resulted in vastly different average saturated hydraulic conductivity (two orders of magnitude) which is ascribed to different averaging volumes as well as various measurement deficiencies such as poor contact, air entrapment, wall artifacts and slaking.

Simulated hydraulic conductivities could be very well predicted with the critical pore diameter for soil samples from the no-till soil cores. However, the predictive power of the critical pore diameter even in combination with other pore structure attributes was very low for cores from the conventionally tilled soil and even lower for measured instead of simulated conductivities due to unavoidable inadequacies in the measurements. Furthermore, the pore space attribute with highest predictive power on hydraulic conductivity changes to macroporosity and pore connectivity in a narrow pressure range (from h=0cm to h=-2cm). This raises the question whether universal pedo-transfer functions for saturated and near-saturated hydraulic conductivities based on X-ray CT derived macropore space properties are promising. It needs to be tested on a larger dataset of structured soil that covers a larger variety of soil textures, bulk densities and macroporosities, which of the investigated pore space attributes (or combinations thereof) is the most robust in predicting (near-)saturated hydraulic conductivity.

Based on these findings we recommend that for constructing pedo-transfer functions for hydraulic conductivity based on structural properties K_{-2} measurements are to be favored over K_s measurements and the measurement technique should always be reported with the actual values when constructing large databases.

6. Acknowledgments

We thank Max Köhne and Eva Lippold for tension infiltrometer measurements, Gick-Mick Wu for assistance with statistics and Hans-Jörg Vogel for in-depth discussions about the manuscript. Hood infiltrometer measurements were done in the frame of a project funded by the German Research Foundation (SCHW1448-6/1).

7. Bibliography

Abdollahi, L., Getahun, G.T., Munkholm, L.J., 2017. Eleven Years' Effect of Conservation Practices for Temperate Sandy Loams: I. Soil Physical Properties and Topsoil Carbon Content. Soil Science Society of America Journal 81(2), 380-391.

Abdollahi, L., Munkholm, L.J., 2017. Eleven Years' Effect of Conservation Practices for Temperate Sandy Loams: Ii. Soil Pore Characteristics. Soil Science Society of America Journal 81(2), 392-403.

Ad-hoc-AG Boden, 2005. Bodenkundliche Kartieranleitung (Ka 5). Schweizerbart, Stuttgart.

Allaire-Leung, S.E., Gupta, S.C., Moncrief, J.F., 2000. Water and Solute Movement in Soil as Influenced by Macropore Characteristics: 1. Macropore Continuity. Journal of Contaminant Hydrology 41(3), 283-301.

Alletto, L., Coquet, Y., 2009. Temporal and Spatial Variability of Soil Bulk Density and near-Saturated Hydraulic Conductivity under Two Contrasted Tillage Management Systems. Geoderma 152(1), 85-94.

Andrä, H., Combaret, N., Dvorkin, J., Glatt, E., Han, J., Kabel, M., Keehm, Y., Krzikalla, F., Lee, M., Madonna, C., Marsh, M., Mukerji, T., Saenger, E.H., Sain, R., Saxena, N., Ricker, S., Wiegmann, A., Zhan, X., 2013. Digital Rock Physics Benchmarks—Part Ii: Computing Effective Properties. Computers & Geosciences 50, 33-43.

Andruschkewitsch, R., Geisseler, D., Koch, H.-J., Ludwig, B., 2013. Effects of Tillage on Contents of Organic Carbon, Nitrogen, Water-Stable Aggregates and Light Fraction for Four Different Long-Term Trials. Geoderma 192, 368-377.

Araya, S.N., Ghezzehei, T.A., 2019. Using Machine Learning for Prediction of Saturated Hydraulic Conductivity and Its Sensitivity to Soil Structural Perturbations. Water Resources Research 55(7), 5715-5737.

Blanco-Canqui, H., Ruis, S.J., 2018. No-Tillage and Soil Physical Environment. Geoderma 326, 164-200.

Blunt, M.J., Bijeljic, B., Dong, H., Gharbi, O., Iglauer, S., Mostaghimi, P., Paluszny, A., Pentland, C., 2013. Pore-Scale Imaging and Modelling. Advances in Water Resources 51, 197-216.

Buczko, U., Bens, O., Hüttl, R.F., 2006. Tillage Effects on Hydraulic Properties and Macroporosity in Silty and Sandy Soils. Soil Science Society of America Journal 70, 1998-2007.

Carsel, R.F., Parrish, R.S., 1988. Developing Joint Probability Distributions of Soil Water Retention Characteristics. Water Resources Research 24(5), 755-769.

Clothier, B.E., Smettem, K.R.J., 1990. Combining Laboratory and Field Measurements to Define the Hydraulic Properties of Soil. Soil Science Society of America Journal 54(2), 299-304.

Dal Ferro, N., Sartori, L., Simonetti, G., Berti, A., Morari, F., 2014. Soil Macro-and Microstructure as Affected by Different Tillage Systems and Their Effects on Maize Root Growth. Soil and Tillage Research 140, 55-65.

Di Prima, S., Marrosu, R., Lassabatere, L., Angulo-Jaramillo, R., Pirastru, M., 2018. In Situ Characterization of Preferential Flow by Combining Plot- and Point-Scale Infiltration Experiments on a Hillslope. Journal of Hydrology 563, 633-642.

Dieckmann, J., 2008. Zur Bedeutung Der Bodenstruktur Für Den Ertrag Von Zuckerrüben – Eine Pflanzenbauliche Und Ökonomische Analyse in Einer Zuckerrüben - Getreide - Fruchtfolge Mit Dauerhaft Differenzierter Bodenbearbeitung, Göttingen University, Göttingen.

Fodor, N., Sándor, R., Orfanus, T., Lichner, L., Rajkai, K., 2011. Evaluation Method Dependency of Measured Saturated Hydraulic Conductivity. Geoderma 165(1), 60-68.

Gardner, W.R., 1958. Some Steady-State Solutions of the Unsaturated Moisture Flow Equation with Application to Evaporation from a Water Table. Soil Science 85(4), 228-232.

Ippisch, O., Vogel, H.-J., Bastian, P., 2006. Validity Limits for the Van Genuchten-Mualem Model and Implications for Parameter Estimation and Numerical Simulation. Advances in Water Resources 29, 1780-1789.

Jacobs, A., Jungert, S., Koch, H.-J., 2015. Soil Organic Carbon as Affected by Direct Drilling and Mulching in Sugar Beet – Wheat Rotations. Archives of Agronomy and Soil Science 61(8), 1079-1087.

Jarvis, N., Koestel, J., Messing, I., Moeys, J., Lindahl, A., 2013. Influence of Soil, Land Use and Climatic Factors on the Hydraulic Conductivity of Soil. Hydrol. Earth Syst. Sci. 17(12), 5185-5195.

Jarvis, N., Larsbo, M., Koestel, J., 2017. Connectivity and Percolation of Structural Pore Networks in a Cultivated Silt Loam Soil Quantified by X-Ray Tomography. Geoderma 287, 71-79.

Jarvis, N.J., 2007. A Review of Non-Equilibrium Water Flow and Solute Transport in Soil Macropores: Principles, Controlling Factors and Consequences for Water Quality. European Journal of Soil Science 58, 523-546.
Jirků, V., Kodešová, R., Nikodem, A., Mühlhanselová, M., Žigová, A., 2013. Temporal Variability of Structure and Hydraulic Properties of Topsoil of Three Soil Types. Geoderma 204-205, 43-58.
Jorda, H., Bechtold, M., Jarvis, N., Koestel, J., 2015. Using Boosted Regression Trees to Explore Key Factors Controlling Saturated and near-Saturated Hydraulic Conductivity. European Journal of Soil Science 66(4), 744-756.
Kahlon, M.S., Lal, R., Ann-Varughese, M., 2013. Twenty Two Years of Tillage and Mulching Impacts on Soil Physical Characteristics and Carbon Sequestration in Central Ohio. Soil and Tillage Research 126, 151-158.
Kang, D.H., Yang, E., Yun, T.S., 2019. Stokes-Brinkman Flow Simulation Based on 3-D M-Ct Images of Porous Rock Using Grayscale Pore Voxel Permeability. Water Resources Research 55(5), 4448-4464.
Katz, A.J., Thompson, A.H., 1986. Quantitative Prediction of Permeability in Porous Rock. Physical Review B 34(11), 8179-8181.
Kaufmann, M., Tobias, S., Schulin, R., 2010. Comparison of Critical Limits for Crop Plant Growth Based on Different Indicators for the State of Soil Compaction. Journal of Plant Nutrition and Soil Science 173(4), 573-583.
Koch, H.-J., Dieckmann, J., Büchse, A., Märländer, B., 2009. Yield Decrease in Sugar Beet Caused by Reduced Tillage and Direct Drilling. European Journal of Agronomy 30(2), 101-109.
Koestel, J., 2018. Soilj: An Imagej Plugin for the Semiautomatic Processing of Three-Dimensional X-Ray Images of Soils. Vadose Zone Journal 17(1).
Koestel, J., Dathe, A., Skaggs, T.H., Klakegg, O., Ahmad, M.A., Babko, M., Giménez, D., Farkas, C., Nemes, A., Jarvis, N., 2018. Estimating the Permeability of Naturally Structured Soil from Percolation Theory and Pore Space Characteristics Imaged by X-Ray. Water Resources Research 54(11), 9255-9263.
Kravchenko, A., Wang, A., Smucker, A., Rivers, M., 2011. Long-Term Differences in Tillage and Land Use Affect Intra-Aggregate Pore Heterogeneity. Soil Science Society of America Journal 75(5), 1658-1666.
Kuhwald, M., Blaschek, M., Brunotte, J., Duttmann, R., 2017. Comparing Soil Physical Properties from Continuous Conventional Tillage with Long-Term Reduced Tillage Affected by One-Time Inversion. Soil Use and Management 33(4), 611-619.
Kuka, K., Illerhaus, B., Fritsch, G., Joschko, M., Rogasik, H., Paschen, M., Schulz, H., Seyfarth, M., 2013. A New Method for the Extraction of Undisturbed Soil Samples for X-Ray Computed Tomography. J. Nondestr. Test. 2013(8).
Larsbo, M., Koestel, J., Jarvis, N., 2014. Relations between Macropore Network Characteristics and the Degree of Preferential Solute Transport. Hydrology and Earth System Sciences 18(12), 5255-5269.
Lebert, M., Brunotte, J., Sommer, C., 2004. Ableitung Von Kriterien Zur Charakterisierung Einer Schädlichen Bodenverdichtung Entstanden Durch Nutzungsbedingte Verdichtung Von Böden/Regelungen Zur Gefahrenabwehr, Umweltbundeamt, Berlin.
Legland, D., Arganda-Carreras, I., Andrey, P., 2016. Morpholibj: Integrated Library and Plugins for Mathematical Morphology with Imagej. Bioinformatics 32(22), 3532-3534.
Licht, M.A., Al-Kaisi, M., 2005. Strip-Tillage Effect on Seedbed Soil Temperature and Other Soil Physical Properties. Soil and Tillage Research 80(1), 233-249.
Linden, S., Wiegmann, A., Hagen, H., 2015. The Lir Space Partitioning System Applied to the Stokes Equations. Graphical Models 82, 58-66.

Lipiec, J., Kuś, J., Słowińska-Jurkiewicz, A., Nosalewicz, A., 2006. Soil Porosity and Water Infiltration as Influenced by Tillage Methods. Soil and Tillage research 89(2), 210-220.
Lucas, M., Schlüter, S., Vogel, H.-J., Vetterlein, D., 2019. Soil Structure Formation Along an Agricultural Chronosequence. Geoderma 350, 61-72.
Matula, S., Miháliková, M., Lufinková, J., Báťková, K., 2015. The Role of the Initial Soil Water Content in the Determination of Unsaturated Soil Hydraulic Conductivity Using a Tension Infiltrometer. Plant, Soil and Environment 61(11), 515-521.
Mevik, B.-H.W., Ron; Liland, Kristian Hovde, 2016. Pls: Partial Least Squares and Principal Component Regression.
Morbidelli, R., Saltalippi, C., Flammini, A., Cifrodelli, M., Picciafuoco, T., Corradini, C., Govindaraju, R.S., 2017. In Situ Measurements of Soil Saturated Hydraulic Conductivity: Assessment of Reliability through Rainfall–Runoff Experiments. Hydrological Processes 31(17), 3084-3094.
Müller, K., Katuwal, S., Young, I., McLeod, M., Moldrup, P., de Jonge, L.W., Clothier, B., 2018. Characterising and Linking X-Ray Ct Derived Macroporosity Parameters to Infiltration in Soils with Contrasting Structures. Geoderma 313, 82-91.
Pagliai, M., Vignozzi, N., Pellegrini, S., 2004. Soil Structure and the Effect of Management Practices. Soil and Tillage Research 79(2), 131-143.
Palm, C., Blanco-Canqui, H., DeClerck, F., Gatere, L., Grace, P., 2014. Conservation Agriculture and Ecosystem Services: An Overview. Agriculture, Ecosystems & Environment 187, 87-105.
Paradelo, M., Katuwal, S., Moldrup, P., Norgaard, T., Herath, L., de Jonge, L.W., 2016. X-Ray Ct-Derived Soil Characteristics Explain Varying Air, Water, and Solute Transport Properties across a Loamy Field. Vadose Zone Journal 15(4).
Perroux, K.M., White, I., 1988. Designs for Disc Permeameters1. Soil Science Society of America Journal 52, 1205-1215.
Peth, S., Horn, R., Beckmann, F., Donath, T., Fischer, J., Smucker, A.J.M., 2008. Three-Dimensional Quantification of Intra-Aggregate Pore-Space Features Using Synchrotron-Radiation-Based Microtomography. Soil Science Society of America Journal 72(4), 897-907.
Pöhlitz, J., Rücknagel, J., Koblenz, B., Schlüter, S., Vogel, H.-J., Christen, O., 2018. Computed Tomography and Soil Physical Measurements of Compaction Behaviour under Strip Tillage, Mulch Tillage and No Tillage. Soil and Tillage Research 175, 205-216.
Pot, V., Peth, S., Monga, O., Vogel, L.E., Genty, A., Garnier, P., Vieublé-Gonod, L., Ogurreck, M., Beckmann, F., Baveye, P.C., 2015. Three-Dimensional Distribution of Water and Air in Soil Pores: Comparison of Two-Phase Two-Relaxation-Times Lattice-Boltzmann and Morphological Model Outputs with Synchrotron X-Ray Computed Tomography Data. Advances in Water Resources 84, 87-102.
Rabot, E., Wiesmeier, M., Schlüter, S., Vogel, H.J., 2018. Soil Structure as an Indicator of Soil Functions: A Review. Geoderma 314, 122-137.
Rasmussen, K., 1999. Impact of Ploughless Soil Tillage on Yield and Soil Quality: A Scandinavian Review. Soil and Tillage Research 53(1), 3-14.
Reichert, J.M., da Rosa, V.T., Vogelmann, E.S., da Rosa, D.P., Horn, R., Reinert, D.J., Sattler, A., Denardin, J.E., 2016. Conceptual Framework for Capacity and Intensity Physical Soil Properties Affected by Short and Long-Term (14 Years) Continuous No-Tillage and Controlled Traffic. Soil and Tillage Research 158, 123-136.
Reichert, J.M., Suzuki, L.E.A.S., Reinert, D.J., Horn, R., Håkansson, I., 2009. Reference Bulk Density and Critical Degree-of-Compactness for No-Till Crop Production in Subtropical Highly Weathered Soils. Soil and Tillage Research 102(2), 242-254.
Renard, P., Allard, D., 2013. Connectivity Metrics for Subsurface Flow and Transport. Advances in Water Resources 51(0), 168-196.

Renard, P., De Marsily, G., 1997. Calculating Equivalent Permeability: A Review. Advances in Water Resources 20(5), 253-278.
Reynolds, W., Elrick, D., 1985. In Situ Measurement of Field-Saturated Hydraulic Conductivity, Sorptivity, and the A-Parameter Using the Guelph Permeameter. Soil Science 140(4), 292-302.
Reynolds, W.D., Bowman, B.T., Brunke, R.R., Drury, C.F., Tan, C.S., 2000. Comparison of Tension Infiltrometer, Pressure Infiltrometer, and Soil Core Estimates of Saturated Hydraulic Conductivity. Soil Science Society of America Journal 64(2), 478-484.
Rienzner, M., Gandolfi, C., 2014. Investigation of Spatial and Temporal Variability of Saturated Soil Hydraulic Conductivity at the Field-Scale. Soil and Tillage Research 135, 28-40.
Rücknagel, J., Rademacher, A., Götze, P., Hofmann, B., Christen, O., 2017. Uniaxial Compression Behaviour and Soil Physical Quality of Topsoils under Conventional and Conservation Tillage. Geoderma 286, 1-7.
Sammartino, S., Lissy, A.-S., Bogner, C., Van Den Bogaert, R., Capowiez, Y., Ruy, S., Cornu, S., 2015. Identifying the Functional Macropore Network Related to Preferential Flow in Structured Soils. Vadose Zone Journal 14(10).
Schaap, M.G., Leij, F.J., van Genuchten, M.T., 2001. Rosetta: A Computer Program for Estimating Soil Hydraulic Parameters with Hierarchical Pedotransfer Functions. Journal of Hydrology 251(3-4), 163-176.
Schaap, M.G., van Genuchten, M.T., 2006. A Modified Mualem–Van Genuchten Formulation for Improved Description of the Hydraulic Conductivity near Saturation. Vadose Zone Journal 5(1), 27-34.
Schindelin, J., Arganda-Carreras, I., Frise, E., Kaynig, V., Longair, M., Pietzsch, T., Preibisch, S., Rueden, C., Saalfeld, S., Schmid, B., 2012. Fiji: An Open-Source Platform for Biological-Image Analysis. Nature methods 9(7), 676-682.
Schlüter, S., Großmann, C., Diel, J., Wu, G.-M., Tischer, S., Deubel, A., Rücknagel, J., 2018. Long-Term Effects of Conventional and Reduced Tillage on Soil Structure, Soil Ecological and Soil Hydraulic Properties. Geoderma 332, 10-19.
Schlüter, S., Leuther, F., Vogler, S., Vogel, H.-J., 2016. X-Ray Microtomography Analysis of Soil Structure Deformation Caused by Centrifugation. Solid Earth 7(1), 129-140.
Schlüter, S., Sheppard, A., Brown, K., Wildenschild, D., 2014. Image Processing of Multiphase Images Obtained Via X-Ray Microtomography: A Review. Water Resources Research 50(4), 3615-3639.
Schmidt, W., Nitzsche, O., Krück, S., Zimmermann, M., 2002. Entwicklung Von Dauerhaft Umweltgerechten Landbewirtschaftungsverfahren Im Sächsischen Einzugsgebiet Der Elbe. Abschlussbericht zum Forschungsvorhaben FKZ 339588.
Schwärzel, K., Punzel, J., 2007. Hood Infiltrometer—a New Type of Tension Infiltrometer. Soil Science Society of America Journal 71(5), 1438-1447.
Schwen, A., Bodner, G., Scholl, P., Buchan, G.D., Loiskandl, W., 2011. Temporal Dynamics of Soil Hydraulic Properties and the Water-Conducting Porosity under Different Tillage. Soil and Tillage Research 113(2), 89-98.
Smet, S., Beckers, E., Plougonven, E., Léonard, A., Degré, A., 2018. Can the Pore Scale Geometry Explain Soil Sample Scale Hydrodynamic Properties? Frontiers in Environmental Science 6(20).
Soane, B.D., Ball, B.C., Arvidsson, J., Basch, G., Moreno, F., Roger-Estrade, J., 2012. No-Till in Northern, Western and South-Western Europe: A Review of Problems and Opportunities for Crop Production and the Environment. Soil and Tillage Research 118, 66-87.
Strudley, M.W., Green, T.R., Ascough, J.C., 2008. Tillage Effects on Soil Hydraulic Properties in Space and Time: State of the Science. Soil and Tillage Research 99(1), 4-48.
Tebrügge, F., Düring, R.-A., 1999. Reducing Tillage Intensity—a Review of Results from a Long-Term Study in Germany. Soil and tillage research 53(1), 15-28.

Tristán-Vega, A., García-Pérez, V., Aja-Fernández, S., Westin, C.-F., 2012. Efficient and Robust Nonlocal Means Denoising of \Mr\ Data Based on Salient Features Matching. Computer Methods and Programs in Biomedicine 105(2), 131-144.

Ulrich, S., Tischer, S., Hofmann, B., Christen, O., 2010. Biological Soil Properties in a Long-Term Tillage Trial in Germany. Journal of Plant Nutrition and Soil Science 173(4), 483-489.

Van Looy, K., Bouma, J., Herbst, M., Koestel, J., Minasny, B., Mishra, U., Montzka, C., Nemes, A., Pachepsky, Y.A., Padarian, J., Schaap, M.G., Tóth, B., Verhoef, A., Vanderborght, J., van der Ploeg, M.J., Weihermüller, L., Zacharias, S., Zhang, Y., Vereecken, H., 2017. Pedotransfer Functions in Earth System Science: Challenges and Perspectives. Reviews of Geophysics 55(4), 1199-1256.

Vereecken, H., Weynants, M., Javaux, M., Pachepsky, Y., Schaap, M.G., Genuchten, M.T.v., 2010. Using Pedotransfer Functions to Estimate the Van Genuchten–Mualem Soil Hydraulic Properties: A Review. Vadose Zone Journal 9(4), 795-820.

Vogeler, I., Rogasik, J., Funder, U., Panten, K., Schnug, E., 2009. Effect of Tillage Systems and P-Fertilization on Soil Physical and Chemical Properties, Crop Yield and Nutrient Uptake. Soil and Tillage Research 103(1), 137-143.

Wen, X.H., Gómez-Hernández, J.J., 1996. Upscaling Hydraulic Conductivities in Heterogeneous Media: An Overview. Journal of Hydrology 183(1-2), 9-23.

Werner, D., Paul, R., 1999. Kennzeichnung Der Verdichtungs-Gefährdung Landwirtschaftlich Genutzter Böden. Wasser und Boden 51(12), 10-14.

Wooding, R.A., 1968. Steady Infiltration from a Shallow Circular Pond. Water Resources Research 4(6), 1259-1273.

Wösten, J.H.M., Pachepsky, Y.A., Rawls, W.J., 2001. Pedotransfer Functions: Bridging the Gap between Available Basic Soil Data and Missing Soil Hydraulic Characteristics. Journal of Hydrology 251(3), 123-150.

Zhang, Y., Schaap, M.G., 2019. Estimation of Saturated Hydraulic Conductivity with Pedotransfer Functions: A Review. Journal of Hydrology 575, 1011-1030.

Zhang, Z., Liu, K., Zhou, H., Lin, H., Li, D., Peng, X., 2019. Linking Saturated Hydraulic Conductivity and Air Permeability to the Characteristics of Biopores Derived from X-Ray Computed Tomography. Journal of Hydrology 571, 1-10.